Electrochemical approach to the surface characterization of mechanochemically synthesized alumina-supported cobalt applicable in glucose sensing

Tihana Mudrinić , Srđan Petrović , Jugoslav Krstić , Biljana Milovanović , Stefan Pavlović , Predrag Banković , Aleksandra Milutinović-Nikolić

PII: S2468-0230(22)00617-4
DOI: https://doi.org/10.1016/j.surfin.2022.102356
Reference: SURFIN 102356

To appear in: *Surfaces and Interfaces*

Received date: 9 March 2022
Revised date: 3 August 2022
Accepted date: 16 September 2022

Please cite this article as: Tihana Mudrinić , Srđan Petrović , Jugoslav Krstić , Biljana Milovanović , Stefan Pavlović , Predrag Banković , Aleksandra Milutinović-Nikolić , Electrochemical approach to the surface characterization of mechanochemically synthesized alumina-supported cobalt applicable in glucose sensing, *Surfaces and Interfaces* (2022), doi: https://doi.org/10.1016/j.surfin.2022.102356

Highlights

- Novel electrochemical approach of alumina-cobalt surface characterization is proven
- Co^{2+}_{Td} was confirmed as main active site in glucose-sensing Co-based electrodes
- Mechanochemistry has great potential for green glucose-sensing material preparation

Electrochemical approach to the surface characterization of mechanochemically synthesized alumina-supported cobalt applicable in glucose sensing

Tihana Mudrinić[1], Srđan Petrović, Jugoslav Krstić, Biljana Milovanović,

Stefan Pavlović, Predrag Banković, Aleksandra Milutinović-Nikolić

Department of Catalysis and Chemical Engineering, University of Belgrade – Institute of Chemistry, Technology and Metallurgy – National Institute of the Republic of Serbia, Belgrade, Republic of Serbia

Abstract

The main goals of this study are: i) employ the electrochemical methods as alternative methods for alumina-supported cobalt (Co-A) surface characterization; ii) investigate the electro-catalytic activity of different cobalt phases toward glucose, and iii) implement the mechanochemical approach for the synthesis of the fourth generation of glucose sensing materials. Co_3O_4 and alumina were either manual grinded (Co_3O_4-A) or ball-milled ($CoAl_2O_4$-A) with different amounts of cobalt in $CoAl_2O_4$-A. The final products were characterized by XRF, LDPSA, XRD and TPR. The electrodes were prepared in the form of the carbon paste electrode and tested in supporting electrolyte (1 M NaOH) as well as in a glucose-containing solution. The CV, EIS, and chronoamperometry were used for electrochemical measurements. TPR revealed the formation of $CoAl_2O_4$ during the ball milling process. Different cobalt phases significantly affected the electrochemical responses. Higher activity of $CoAl_2O_4$-A toward glucose oxidation in comparison with Co_3O_4-A was ascribed to tetrahedral Co^{2+} ion acting as the active site in glucose oxidation. In addition, results convinced employing the scarcely employed mechanochemical synthesis protocols for obtaining glucose-sensing materials. Finally, it was proven that electrochemical techniques can be harnessed as alternative, new, powerful methods for Co-A surface characterization.

[1] Corresponding author: tihana@nanosys.ihtm.bg.ac.rs; tihana.mudrinic@ihtm.bg.ac.rs;
Phone: (+381)-11-2630-213;Fax: (+381)-11-2637-977.

Keywords: glucose sensing, cobalt-alumina, mechanochemistry, electrochemistry

1. Introduction

In recent years, mineral oxides (such as alumina and clay)-supported cobalt (Co-MO) have been extensively studied as a cheaper and eco-friendly alternative to noble metal-based (electro)catalysts [1–8]. Such interest rose from the fact that Co-MO exhibited many desirable catalytic properties and in the same time fulfill the contemporary requests for using sustainable green materials.

Further research efforts to find environmentally-benign preparation techniques in catalysts synthesis represent another focus. In this regard, the mechanochemical method of synthesis [3,4,9,10] emerged as a highly promising method. Besides avoiding toxic chemicals, the mechanochemical approach also provides avoidance of time-consuming process steps (i.e. filtration, pH controlling, washing, and calcination) as well as obtaining catalysts with properties that are difficult to achieve through conventional solvent-based methods [11,12].

The main characteristic of Co-MO is the interaction between cobalt and mineral oxides [5,13,14]. This interaction causes a significant change in the surface of the catalysts by forming different cobalt phases (i.e. Co_3O_4 and $CoAl_2O_4$). The relative distribution of these cobalt phases is significantly influenced by the synthesis process parameters [14] (i.e metal loading and calcination temperature) and crystallographic forms of alumina [6,15]. Several studies disclosed that the relative distribution of the cobalt oxides strongly affects the catalytic activity of alumina-supported cobalt catalysts (Co-A). For example, Co_3O_4 is regarded as an active site for the Fisher-Tropsch process, whereas the $CoAl_2O_4$ is almost inactive [14]. In the light of recent findings, the difference in catalytic activity between these two forms of cobalt oxides could be interpreted in terms of the differences in the catalytic activity of cobalt ions [16–19]. This can be explained by the fact that the Co_3O_4 contains both tetrahedral ($Co^{2+}{}_{Td}$) and octahedral ($Co^{3+}{}_{Oh}$) cobalt ions, while the $CoAl_2O_4$ is composed of $Co^{2+}{}_{Td}$. Numerous reports revealed that $Co^{2+}{}_{Td}$ and $Co^{3+}{}_{Oh}$ differ from each other in catalytic activity. Thus, $Co^{3+}{}_{Oh}$ is considered as the active site for CO oxidation [20], while it is relatively inactive towards oxygen evolution reaction (OER) [18] and oxygen reduction reaction (ORR) [16]. These findings indicate that there is no universal surface characteristic of Co-A which would be active in all catalytic reactions. Accordingly, there is no doubt that the surface science studies of the Co-A are of crucial importance to tailor the catalysts with desired properties as well as for an in-depth understanding of their catalytic performance.

In the literature, a variety of techniques have been employed concerning the surface characterization of Co-A including various spectroscopic techniques [13] and temperature-programmed reduction [14]. Since the surface of Co-A is very sensitive to the synthesis process parameters; it would be very advantageous to have a low-cost, rapid assay for its characterization during optimization.

Although the cobalt-based electrodes were employed to investigate various electrochemical reactions (ORR [16], OER [18,19] and glucose detection [21], to the best of our knowledge, electrochemical techniques were not employed to characterize cobalt-alumina interactions. Therefore, one of the goals of the present study was to employ the electrochemical techniques as a less time consuming and cumbersome approach to obtain information of different cobalt phases supported on alumina.

Other goals of the present work were directed in further development of modern non-enzymatic and noble-free glucose sensors based on mineral oxides [8,22,23]. Although the great achievement (i.e. high sensitivity and accuracy, as well as adequate response range) has been obtained, further research and detailed understanding of these materials are needed. For instance, the effect of the main feature of the Co-A i.e. cobalt-alumina interaction on the electrooxidation of glucose has been remained unclear. Moreover, despite many advantages of the mechanochemical synthesis protocols, mechanochemical synthesized materials based on Co-MO were not employed in glucose-sensing.

Therefore, in this work, two types of Co-A with different cobalt phases were prepared by grinding of Co_3O_4 and alumina: manually in an agate mortar (Co_3O_4-A), and mechanochemically using a planetary ball mill ($CoAl_2O_4$-A). The prepared catalysts were tested in alkaline solution with and without glucose using cyclic voltammetry, chronoamperometry, and electrochemical impedance spectroscopy. The electrochemical results taken together with the physical-chemical characterization of the synthesized materials are used to provide valuable insights into i) the possibility of using electrochemical techniques for surface characterization of Co-A; ii) electrocatalytic activity of different cobalt phases toward glucose oxidation, and iii) possible employing the low cost and scalable synthesis protocols to obtained glucose-sensing materials.

2. Materials and methods

2.1. Catalyst preparation

Mechanochemical preparation of samples was carried out in the planetary ball mill RETSCH, PM 100 using a stainless milling jar and balls. Appropriate amounts of alumina (Metallurgical alumina type SANDY, "Alumina" d.o.o Zvornik [24] and Co_3O_4 (Merck) were mixed to synthesize the electrocatalysts with (4, 8 and 16) mass % of Co_3O_4 content. The ball-to-powder mixture ratio was constant, 30:1. Milling was conducted at 300 rpm for 60 min using a stainless steel jar and balls in reverse motion mode. Mechanochemically prepared samples were denoted as x%$CoAl_2O_4$-A where x=4, 8, 16 represents the weight percentage of introduced Co_3O_4. Catalyst (4%Co_3O_4-A) was prepared by manual grinding of 4 mass % of Co_3O_4 and alumina in an agate mortar.

2.2. Characterization of synthesized materials

The chemical composition of alumina and synthesized samples was analyzed using the X-ray fluorescence analysis equipment (EDX-8000 energy dispersive X-ray fluorescence spectrometer, Shimadzu). The identification of a crystalline structure was carried by X-ray diffractometry (XRD, Bruker D8 Endeavor diffractometer) over the angular range of 10-90° (2θ) at a scanning rate 1 ° min^{-1} with a step size of 0.02°, using CoKα radiation (λ=0.178896 nm). The powder size was assessed by a Cilas 1090 laser diffraction particle size analyzer (LDPSA). Cobalt oxides reducibility was evaluated by the temperature-programmed reduction (TPR) using a TPDRO 11000 Thermo Finningen. The TPR experiments were conducted using a 4.9% H_2/Ar gas mixture with a flow rate of 20 cm^3 min^{-1}. The temperature was linearly raised from 40 to 900 °C at the heating rate of 10 °C min^{-1}. A trap filled with $CaO+NaO+Mg(ClO_4)_2$ was installed between the oven and thermal conductivity detector (TCD) to remove H_2O and CO_2, formed during the reduction.

2.3. Preparation of modified carbon paste electrode

Modified carbon black paste was prepared by hand mixing of each of prepared catalysts (section 2.1.) and carbon black (CB) (Vulcan-XC 72R) with paraffin oil and denoted as CP-4%Co_3O_4-A and CP-x%$CoAl_2O_4$-A. The carbon paste electrode modified with alumina (CP-Al_2O_3) without cobalt was also prepared for comparison purpose. The resulting paste was packed into the hollow (2 mm diameter) Teflon tube, while the electrical contact was provided using copper wire and the obtained setup was used as working electrode. The mass ratio of the catalyst and CB was 50:50.

2.4. Electrochemical measurements on modified carbon paste electrodes

The electrochemical measurements were performed using Autolab Electrochemical Workstation (Autolab PGSTAT302 N, Metrohm- Autolab BV, Netherlands). The electrochemical cell consisted of a three-electrode system. The prepared electrodes were used as working electrode, Ag/AgCl in 3M KCl as the reference electrode, while a platinum rod served as a counter electrode. The pure carbon black paste electrode was tested in our previous work [8]. Cyclic voltammetry (CV) was carried out in the potential range from -0.20 V to +0.65 V in 1 M NaOH solution with and without glucose. Chronoamperometry was performed by applying +0.45 V to the working electrode. Before the addition of the glucose in NaOH solution the stable constant current of the background of NaOH solution was reached. The solution was constantly stirred using a magnetic stirrer.

Electrochemical impedance spectroscopy (EIS) was carried out at +0.4 V in 1 M NaOH using a 10 mV RMS sinusoidal modulation in the $1 \cdot 10^5$ Hz – 0.1 Hz frequency range.

3. Results and discussion

3.1. Results of material characterization

The results of the X-ray fluorescence spectroscopy analysis (Table 1) are given for main elements.

Table 1. Chemical composition of samples.

Sample	Oxide content (mass %)		Element content (mass %)			
	$Co_3O_{4theor.}$	$Co_{theor.}$	Al	Fe	Co	O
Al_2O_3	-	-	52.84	0.01	0.00	47.16
4%$CoAl_2O_4$-A	4.0	2.94	50.09	0.68	3.08	46.15
8%$CoAl_2O_4$-A	8.0	5.87	48.09	0.26	6.12	45.52
16%$CoAl_2O_4$-A	16.0	11.75	46.45	0.14	11.92	41.50

The introduction of commercial Co_3O_4 into alumina by mechanochemical grinding resulted in an increase in cobalt content and a relative decrease in the content of aluminum. With the introduction of cobalt this trend was more pronounced. The amount of theoretically calculated cobalt content ($Co_{theor.}$) is somewhat lower than experimentally obtained values, probably since the commercial powder of Co_3O_4 contains crystalographically confirmed (Fig. 1) CoO. Nevertheless, the measured cobalt content values are in very good agreement with the theoretically calculated ones. The observed increase of Fe content can be attributed to slight derogation of steel balls used in the grinding process.

The particle size distribution (PSD) of the synthesized samples is presented in Fig. 1. In Fig. 1a, the comparative particle size distributions for the initial oxides Co_3O_4 and Al_2O_3 is given, while the effect of mechanochemical grinding is presented in Fig. 1b. The results presented in Fig. 1 are given in Table 2 in percentile form.

Fig. 1

It can be seen that the starting oxides have different granulation and that monomodal distributions with a predominant particle size of 0.59 μm and 85.1 μm for Co_3O_4 and Al_2O_3, respectively, were found. Grinding in a planetary mill for 60 min led to a change in particle distribution width and is different for different concentrations of cobalt oxide in the mixture. A bimodal distribution of the curves of milled samples with broad peaks was observed. The bimodal PSD is caused by the introduction of smaller Co_3O_4 particles onto Al_2O_3. The moderate slope of the cumulative curve for mechanochemically treated samples in comparison with Al_2O_3 indicated that a wide range of particle size was produced during

grinding caused by fracturing of Al_2O_3 particles. It should be pointed out that particle size decreased with metal oxide loading (Table 2), which indicated that Co_3O_4 particles were not subjected to agglomeration. The crushed alumina might provide enough anchoring sites to prevent the agglomeration of Co_3O_4. In that manner, it indicates that dispersed Co_3O_4 over alumina could be obtained by the mechanochemical method even for large metal oxide loadings without agglomeration. Thus, the maximum distribution for small particles is around 2 μm, while the maximum for larger particles shifts towards lower values at 62.6 μm → 32.7 μm → 30.3 (52.4) μm with the increase of cobalt oxide content 4%$CoAl_2O_4$-A→ 8%$CoAl_2O_4$→ 16%$CoAl_2O_4$-A, respectively (Fig. 1b).

Table 2. Percentile values d_{10}, d_{50}, and d_{90} were obtained from the cumulative distribution curve for starting oxides and samples after mechanochemical treatment.

Sample	Particle size (μm)		
	d_{10}	d_{50}	d_{90}
Al_2O_3	27.27	69.66	125.87
Co_3O_4	/	1.20	/
4%$CoAl_2O_4$-A	1.12	29.92	121.17
8%$CoAl_2O_4$-A	0.88	16.71	76.43
16%$CoAl_2O_4$-A	0.5	10.57	69.54

Where d_{10}, d_{50} and d_{90} are the particle diameters at 10%, 50% and 90% in the cumulative distribution.

The X-ray powder diffraction patterns of starting oxides are presented in Fig. 2. The starting commercial alumina is a mixture of the trigonal form with lattice parameters *a*=0.475 nm and *c*=1.296 nm and monoclinic with calculated values of unit cell parameters of *a*=1.185 nm, *b*=0.290 nm, *c*=0.562 nm and *β*=103.8° [25]. The XRD of commercial cobalt oxide powder used in this work also represents a mixture of oxides, more precisely CoO [26] and Co_3O_4 [27], and the characteristic reflections are indicated in Fig. 2.

Fig. 2

Fig. 3a shows the results of XRD analysis of powder samples after mechanochemical treatment for 60 min. The XRD analysis showed the presence of characteristic reflections of the starting alumina, as expected, because it is present in a large excess. Trigonal Al_2O_3 continues to be the dominant phase. The phase $CoAl_2O_4$ may also exist. Namely, both Co_3O_4 and $CoAl_2O_4$ crystallize in the spinel form. X-ray analysis cannot distinguish these phases due to overlapping peaks [27,28], so it is not possible to determine to what extent cobalt

reacted with Al_2O_3, but it is certain that this reaction occurred to a certain extent. It is most likely that the cobalt from Co (II) oxide reacted with aluminum oxide to form a spinel form of $CoAl_2O_4$. The increase in peak intensity at 43º 2θ (Fig. 3b) corresponds to an increase in cobalt content in spinel form. Based on the XRD results, it is not possible to precisely determine the extent to which the $CoAl_2O_4$ and Co_3O_4 phases are present.

Fig. 3

The TPR profiles of the investigated samples are depicted in Fig. 4. Peaks can be observed only on TPR profiles of cobalt-containing samples, while Al_2O_3 could be considered as non-reducible within the studied temperature window. Hence, the observed peaks could be exclusively assigned to the reduction of the cobalt oxides.-At low temperatures (250-500 °C), Co_3O_4-A exhibited only one peak, which can be attributed to easily reducible Co_3O_4 [14]. The x%$CoAl_2O_4$-A exhibited two additional broad peaks at higher temperatures, aside from the low-temperature one. The peak between (500-800) °C was attributed to the presence of some kind of intermediate structure with strong interaction between cobalt (most probably Co^{2+}) and Al_2O_3, whereby the spinel structure was not fully formed [29]. The peak that emerged above 800 °C could be attributed to the formation of the spinel phase i.e. $CoAl_2O_4$ [14,29]. Although the complete reduction of $CoAl_2O_4$ is not reached even for the highest applied temperature, the relative ratio of TPR peaks of x%$CoAl_2O_4$-A increased with the increase of cobalt loading.

Fig. 4

3.2. *Electrochemical behavior in supporting electrolyte*

The electrochemical behavior of CP-Al_2O_3, CP-4%Co_3O_4-A and CP-4%$CoAl_2O_4$-A is investigated by cyclic voltammetry in 1 M NaOH. Stable cyclic voltammograms (CV) of investigated electrodes are compared in Fig. 5a.

Fig.5

No obvious peaks were observed at CP-Al_2O_3. Contrary, CP-4%Co_3O_4-A and CP-4%$CoAl_2O_4$-A displayed well-defined redox peaks attributed to the conversion between different oxidation states of cobalt (Fig 5a). In particular, the CP-4%Co_3O_4-A (black solid line) exhibited two oxidation peaks (A1/A2 and A3) in the positive-going scan and three cathodic peaks (C1, C2 and C3) in the negative-going scan. According to the literature data

[30], the oxidation peak A1/A2 was assigned to overlapped peaks corresponding to peaks C1 and C2 and can be attributed to the Co(II)/Co_3O_4 and Co_3O_4/CoOOH redox couples, respectively. Further, peak A3 and corresponding C3 can be attributed to the CoO_2/CoOOH redox couple [21]. On the other hand, CV of CP-4%$CoAl_2O_4$-A (gray line) revealed that ball milling of Al_2O_3 in the presence of Co_3O_4 introduced interesting changes in electrochemical behavior in comparison with manually grinded samples. This difference is illustrated as the difference between Figs. 5b and 5c. Unlike CP-4%Co_3O_4-A (Fig. 5b), CP-4%$CoAl_2O_4$-A (Fig. 5c) exhibited a significant difference between the first and the stable CV (obtained after 2 cycles). Furthermore, the significant shift of peak A1/A2 and peak C1 towards lower potential (around 0.1 V) was accompanied with dramatic decline in the peaks of A3 and C3 intensities (Fig.5 c). The absence of A3 follows the earlier observation of Wang et al. [18]. They suggested that the aluminum substituent in $CoAl_2O_4$ could either affect the kinetics of oxidation of cobalt and hence causing the shift of the peak potential after OER current, or the kinetics of oxidation of cobalt could be masked by double-layer capacitance.

The present study revealed that the observed negative shift of peaks of CP-4%$CoAl_2O_4$-A in comparison to CP-4%Co_3O_4-A (Fig. 5a) is well correlated with the appearance of high-temperature TPR peaks (Fig. 4) and could be ascribed to the cobalt phase, which has a lower tendency to get reduced, i.e., $CoAl_2O_4$. It should be pointed out that stable CV were obtained after the second cycle. Drawing a parallel with the results of TPR, where the peak between 500-800 °C was attributed to the presence of an intermediate structure with strong interaction between Co^{2+} and Al_2O_3, it can be assumed that, probably during the first CV cycle, the permanent change of this intermediate structure occurred.

Fig. 6 shows stable cyclic voltammograms for electrodes modified with samples with different cobalt content (CP-x%$CoAl_2O_4$-A) recorded in 1 M NaOH solution.

Fig.6

All CP-x%CoAP electrodes displayed the same above-described behavior. In stable cyclic voltammograms of all mechanochemically obtained samples, only one pair of peaks at approx. 0.1 V was registered and could be assigned to overlapped peaks corresponding to Co(II)/Co_3O_4 and Co_3O_4/CoOOH redox couples. Cyclic voltammograms at different scan rates (not shown) were recorded in order to unambiguously determinate the reversibility of the processes at the electrode/electrolyte interface. The overall oxidation-reduction processes

are electrochemically quasi-reversible since the peak potentials slightly drifted apart as a function of the scan rate.

Differences between the CV of samples with different cobalt oxide loadings are only in the current intensity. These results are in accordance with the results of granulometric measurements that revealed the high distribution of cobalt oxide over alumina even for large cobalt loading without agglomeration. Therefore, the higher current intensities corresponded to the presence of more cobalt active sites.

Further characterization of the surface of CP-4%Co_3O_4-A and CP-4%$CoAl_2O_4$-A was performed by EIS in the solution of 1 M NaOH. The recorded Bode plots are presented in Fig. 7.

Fig. 7

The impedance spectrum of CP-4%Co_3O_4-A exhibited two phase relaxation peaks, one less expressed in the low-frequency region and the other in the high-frequency region. By contrast, only one phase relaxation peak was observed for CP-4%$CoAl_2O_4$-A in the low-frequency region. According to the work of Wang et al. [18], the high-frequency peak could be ascribed to the presence of $Co^{3+}{}_{Oh}$, while the low frequency peak could be ascribed to $Co^{2+}{}_{Td}$. The appearance of two phase relaxation peaks for CP-4%Co_3O_4-A well agrees with the presence of Co_3O_4, which contains of two cobalt ions: $Co^{2+}{}_{Td}$ and $Co^{3+}{}_{Oh}$ on alumina. On the other hand, the appearance of only one low-frequency phase peak for CP-4%$CoAl_2O_4$-A indicated that the mechanochemically synthesized sample contained the most dominant $Co^{2+}{}_{Td}$ phase. These results follow the results of TPR measurements (Fig.4), which indicated that cobalt predominately occurred in the Co^{2+} oxidation state in 4%$CoAl_2O_4$-A. All the above discussion about the electrochemical measurements discloses the usefulness of the electrochemical techniques in the analysis of the surface of the Co-A.

3.3. *Electrochemical behavior in glucose containing solution*

Cyclic voltammetry recorded in a glucose-containing solution showed that all investigated electrodes, except pure alumina and bare CB (published in ref [8]), were active toward glucose oxidation (Fig. 8).

Fig. 8

CV showed that the oxidation peak of glucose appeared at +0.45 V. According to literature [21], the mechanism of glucose oxidation on the Co_3O_4 electrode in alkaline solution can be expressed by the following equations:

$$Co_3O_4 + OH^- + H_2O \rightarrow 3CoOOH + e^- \quad (1)$$

$$CoOOH + OH^- \rightarrow CoO_2 + H_2O + e^- \quad (2)$$

$$2CoO_2 + C_6H_{12}O_6 \rightarrow 2CoOOH + C_6H_{10}O_6 \quad (3)$$

The mechanism involves oxidation of Co_3O_4 to CoO_2 in the presence of OH^- ion (Eq. 1 and Eq. 2). Further, the generated CoO_2 oxidized glucose to gluconolactone and CoOOH (Eq. 3). The increase of CoOOH content favors the Eq. 2 causing the increase of the current peak at +0.45 V (peak denoted as A3 in Fig. 5a) upon the addition of glucose into an alkaline solution.

Differences in electrocatalytic activity between CP-4%Co_3O_4-A and CP-4%$CoAl_2O_4$-A in the reaction of electrooxidation of glucose were also investigated using the chronoamperometric method in order to compare the sensitivity of these electrodes. Chronoamperometry was performed in 1 M NaOH at +0.45 V for glucose concentration range up to 18 mM. It should be noted that all investigated electrodes were cycled in 1 M NaOH to reach stable CV before chronoamperometric measurements. Chronoamperometric responses and corresponding calibration curves are depicted in Fig. 9. Langmuir equation [21] (Eq. 4) was the one that had the best fit to experimental data with R^2=0.99.

$$I = \frac{KC_{glucose}}{1+K_A C_{glucose}} \quad (4)$$

Where: $K = K_A K_B C_t$ and K_A – adsorption equilibrium constant, K_B – rate constant of glucose adsorption on the catalytic surface, C_t is the total molar concentration of active sites on electrode surface, and $C_{glucose}$ – concentration of glucose in the bulk electrolyte.

Fig. 9

For low glucose concentration, $K_A C_{glucose} \ll 1$ and the Eq. 4 can be approximated with $I = KC_{glucose}$. Therefore, a low glucose concentration region was used to estimate the sensitivity of the investigated electrodes. There is a difference in values of sensitivity for CP-4%Co_3O_4-A (17.8 μA mM^{-1} cm^{-2}) and CP-4%$CoAl_2O_4$-A (27.8 μA mM^{-1} cm^{-2}), Table 3. Taking into account the results of TPR (Fig. 4) and EIS (Fig. 6), which disclosed that CP-4%$CoAl_2O_4$-A

predominantly contains tetrahedral Co^{2+} (Co^{2+}_{Td}), while CP-4%Co_3O_4-A contains a mixture of Co^{2+}_{Td} and octahedral Co^{3+} (Co^{3+}_{Oh}), it can be concluded that the Co^{2+}_{Td} is responsible for the oxidation of glucose. These findings seem to be consistent with research of Wang et al. [18], which found that Co^{3+}_{Oh} is relatively inactive in comparison to Co^{2+}_{Td} in Co_3O_4 in the formation of CoOOH, which is essential in the glucose oxidation mechanism (Eqs. 1-3).

Increasing of cobalt loading resulted in an increase in the response toward glucose (Fig. 10 and Table 3). This finding is in accordance with results of behavior in supporting electrolyte, which is attributed to a good distribution of high content of cobalt-phase onto alumina favored by the mechanochemical grinding process.

Fig. 10.

Table 3. Parameters of Langmuir fitting curves of the investigated electrodes.

Electrode	**K**	**K_A**	**R^2**	**Sensitivity (μA mM^{-1} cm^{-2})**
CP-4%Co_3O_4-A	0.56	0.068	0.993	17.8
CP-4%$CoAl_2O_4$-A	0.87	0.091	0.993	27.8
CP-8%$CoAl_2O_4$-A	1.37	0.109	0.994	43.7
CP-16%$CoAl_2O_4$-A	2.45	0.116	0.987	77.9

Conclusion

Commercial Co_3O_4 and Al_2O_3 were used as precursors for preparing two types of alumina-supported cobalt catalysts (Co-A). An agate mortar with a pestle were used to manually crush the precursors into Co_3O_4-A, while a planetary ball mill was used to mechanochemically obtain $CoAl_2O_4$-A. Different amounts of Co_3O_4 were applied in mechanochemical grinding, resulting in a series of materials with different cobalt loadings.

The incorporation of cobalt into alumina was confirmed using the XRD and TPR techniques. Moreover, it was confirmed that the increase in the introduced amount of the Co_3O_4 precursor led to increasing cobalt species content in the $CoAl_2O_4$-A series. The results of the laser diffraction particle size analysis revealed a high dispersion of cobalt oxide over alumina, even for the largest metal oxide loading without agglomeration. The TPR results showed that Co_3O_4 mainly remained untransformed upon grinding in the agate mortar. However, according to the TPR data, it was confirmed that the cobalt aluminate phases were formed to a certain extent in all $CoAl_2O_4$-A materials.

The electrochemical tests conducted in the supporting electrolyte (1 M NaOH) showed that the type of Co-A has a significant impact on the cyclic voltammetry (CV) and electrochemical impendance spectroscopy (EIS) electrochemical responses of modified carbon paste (CP) electrodes. Well-defined redox peaks, attributed to the conversions between different oxidation states of cobalt, were registered for all investigated electrodes using CV. The difference in the peak positions between CP-Co_3O_4-A and CP-$CoAl_2O_4$-A was significant. In addition, only $CoAl_2O_4$-A exhibited a significant difference between the first and the stable CV (obtained after 2 cycles). The EIS method corroborated the TPR results, confirming that tetrahedral $Co^{2+}{}_{Td}$ is the species dominantly present in $CoAl_2O_4$-A, while two cobalt ions ($Co^{2+}{}_{Td}$ and $Co^{3+}{}_{Oh}$) were found in Co_3O_4-A. These findings support the initial hypothesis of this work that it is possible to employ electrochemical techniques as alternative methods for the Co-A surface characterization. A part of an ongoing follow-up investigation suggests with a high likeliness that the hypothesis is right.

The results of chronoamperometry showed that there are differences in the electrocatalytic activity and sensitivity of different cobalt phases toward glucose in alkaline solution. Moreover, these results revealed that the electrocatalytic activity of the cobalt-based catalysts rather relies on the tetrahedral Co^{2+} than on the octahedral Co^{3+} species. A higher electrocatalytic activity of the mechanochemically obtained $CoAl_2O_4$-A in the process of glucose electrooxidation, led to the conclusion that the mechanochemical approach should be more widely employed in order for green and sustainable glucose-sensing materials of the fourth generation to be obtained.

Credit author statement

Tihana Mudrinić: Conceptualization, Methodology, Visualization, Writing – Original Draft, Writing - Review & Editing, Supervision; **Srđan Petrović:** Conceptualization, Investigation, Visualization, Writing – Original Draft, Writing – Review & Editing; **Jugoslav Krstić:** Investigation, Writing - Review & Editing; **Biljana Milovanović:** Investigation; **Stefan Pavlović:** Investigation; **Predrag Banković:** Writing - Review & Editing, Project administration, **Aleksandra Milutinović-Nikolić:** Conceptualization, Visualization, Writing – Review & Editing.

Declaration of interests

☒The authors declare that they have no known competing financial interests or personal relationships that could have appeared to influence the work reported in this paper.

Acknowledgment

This work was financially supported by the Ministry of Education, Science and Technological Development of the Republic of Serbia (Grant No. 451-03-68/2022-14/200026).

References

[1] S. Marinović, T. Mudrinić, B. Dojčinović, T. Barudžija, P. Banković, T. Novaković, Cobalt-doped alumina catalysts in catalytic oxidation of tartrazine induced by Oxone®, J. Environ. Chem. Eng. 9 (2021) 106348. https://doi.org/10.1016/j.jece.2021.106348.

[2] M. Marković, S. Marinović, T. Mudrinić, M. Ajduković, N. Jović-Jovičić, Z. Mojović, J. Orlić, A. Milutinović-Nikolić, P. Banković, Co(II) impregnated Al(III)-pillared montmorillonite–Synthesis, characterization and catalytic properties in Oxone® activation for dye degradation, Appl. Clay Sci. 182 (2019). https://doi.org/10.1016/j.clay.2019.105276.

[3] M. Lu, N. Fatah, A.Y. Khodakov, New shearing mechanical coating technology for synthesis of alumina-supported cobalt Fischer–Tropsch solid catalysts, J. Mater. Chem. A. 5 (2017) 9148–9155. https://doi.org/10.1039/C7TA01174A.

[4] A. Pineda, M. Ojeda, A.A. Romero, A.M. Balu, R. Luque, Mechanochemical synthesis of supported cobalt oxide nanoparticles on mesoporous materials as versatile bifunctional catalysts, Microporous Mesoporous Mater. 272 (2018) 129–136. https://doi.org/10.1016/j.micromeso.2018.06.029.

[5] M. Schubert, S. Pokhrel, A. Thomé, V. Zielasek, T.M. Gesing, F. Roessner, L. Mädler, M. Bäumer, Highly active Co–Al2O3-based catalysts for CO2 methanation with very low platinum promotion prepared by double flame spray pyrolysis, Catal. Sci. Technol. 6 (2016) 7449–7460. https://doi.org/10.1039/C6CY01252C.

[6] E. Rytter, Ø. Borg, B.C. Enger, A. Holmen, α-alumina as catalyst support in Co Fischer-Tropsch synthesis and the effect of added water; encompassing transient effects, J. Catal. 373 (2019) 13–24. https://doi.org/10.1016/j.jcat.2019.03.013.

[7] B. Jongsomjit, J. Panpranot, J.G. Goodwin, Co-Support Compound Formation in Alumina-Supported Cobalt Catalysts, J. Catal. 204 (2001) 98–109. https://doi.org/10.1006/jcat.2001.3387.

[8] T. Mudrinić, S. Marinović, A. Milutinović-Nikolić, N. Jović-Jovičić, M. Ajduković, Z. Mojović, P. Banković, Novel non-enzymatic glucose sensing material based on pillared clay modified with cobalt, Sensors Actuators, B Chem. 299 (2019).

https://doi.org/10.1016/j.snb.2019.126976.

[9] A. Pineda, A.M. Balu, J.M. Campelo, A. Romero, D. Carmona, F. Balas, J. Santamaría, R. Luque, A dry milling approach for the synthesis of highly active nanoparticles supported on porous materials., ChemSusChem. 4 11 (2011) 1561–1565. https://doi.org/10.1002/cssc.201100265.

[10] M. Lu, N. Fatah, A.Y. Khodakov, Optimization of solvent-free mechanochemical synthesis of Co/Al2O3 catalysts using low- and high-energy processes, J. Mater. Sci. 52 (2017) 12031–12043. https://doi.org/10.1007/s10853-017-1299-8.

[11] C. Xu, S. De, A.M. Balu, M. Ojeda, R. Luque, Mechanochemical synthesis of advanced nanomaterials for catalytic applications, Chem. Commun. 51 (2015) 6698–6713. https://doi.org/10.1039/C4CC09876E.

[12] R.H. Blackmore, M.E. Rivas, T. Eralp Erden, T. Dung Tran, H.R. Marchbank, D. Ozkaya, M. Briceno De Gutierrez, A. Wagland, P. Collier, P.P. Wells, Understanding the mechanochemical synthesis of the perovskite LaMnO3 and its catalytic behaviour, Dalt. Trans. 49 (2019) 232–240. https://doi.org/10.1039/c9dt03590g.

[13] R.L. Chin, D.M. Hercules, Surface spectroscopic characterization of cobalt-alumina catalysts, J. Phys. Chem. 86 (1982) 360–367. https://doi.org/10.1021/j100392a016.

[14] W.-J. Wang, Y.-W. Chen, Influence of metal loading on the reducibility and hydrogenation activity of cobalt/alumina catalysts, Appl. Catal. 77 (1991) 223–233. https://doi.org/10.1016/0166-9834(91)80067-7.

[15] R. Munirathinam, D. Pham Minh, A. Nzihou, Effect of the Support and Its Surface Modifications in Cobalt-Based Fischer–Tropsch Synthesis, Ind. Eng. Chem. Res. 57 (2018) 16137–16161. https://doi.org/10.1021/acs.iecr.8b03850.

[16] J. Xiao, Q. Kuang, S. Yang, F. Xiao, S. Wang, L. Guo, Surface Structure Dependent Electrocatalytic Activity of Co3O4 Anchored on Graphene Sheets toward Oxygen Reduction Reaction, Sci. Rep. 3 (2013) 2300. https://doi.org/10.1038/srep02300.

[17] T.W. Kim, M.A. Woo, M. Regis, K.-S. Choi, Electrochemical Synthesis of Spinel Type ZnCo2O4 Electrodes for Use as Oxygen Evolution Reaction Catalysts, J. Phys. Chem. Lett. 5 (2014) 2370–2374. https://doi.org/10.1021/jz501077u.

[18] H.-Y. Wang, S.-F. Hung, H.-Y. Chen, T.-S. Chan, H.M. Chen, B. Liu, In Operando Identification of Geometrical-Site-Dependent Water Oxidation Activity of Spinel Co3O4, J. Am. Chem. Soc. 138 (2016) 36–39. https://doi.org/10.1021/jacs.5b10525.

[19] Y. Xu, F. Zhang, T. Sheng, T. Ye, D. Yi, Y. Yang, S. Liu, X. Wang, J. Yao, Clarifying the controversial catalytic active sites of Co3O4 for the oxygen evolution reaction, J. Mater. Chem. A. 7 (2019) 23191–23198. https://doi.org/10.1039/C9TA08379K.

[20] X. Xie, Y. Li, Z.-Q. Liu, M. Haruta, W. Shen, Low-temperature oxidation of CO catalysed by Co3O4 nanorods, Nature. 458 (2009) 746–749. https://doi.org/10.1038/nature07877.

[21] Y. Ding, Y. Wang, L. Su, M. Bellagamba, H. Zhang, Y. Lei, Electrospun Co3O4 nanofibers for sensitive and selective glucose detection, Biosens. Bioelectron. 26 (2010) 542–548. https://doi.org/10.1016/j.bios.2010.07.050.

[22] S.K. Hassaninejad–Darzi, M. Rahimnejad, S.N. Mirzababaei, Electrocatalytic oxidation of glucose onto carbon paste electrode modified with nickel hydroxide decorated NaA nanozeolite, Microchem. J. 128 (2016) 7–17. https://doi.org/https://doi.org/10.1016/j.microc.2016.03.016.

[23] M. Li, S. Xu, F. Ni, Y. Wang, S. Chen, L. Wang, Fast and sensitive non-enzymatic glucose concentration determination using an electroactive anionic clay-modified electrode, Microchim. Acta. 166 (2009) 203–208. https://doi.org/10.1007/s00604-009-0189-4.

[24] "Alumina" d.o.o,. https://www.aluminazv.ba/en/category-products/8 (accessed February 4, 2003).

[25] (COD ID: 1000017) V.G.- Tsirelson, M. Yu. Antipin, R.G. Gerr, R.P. Ozerov, Y.T. Struchkov, Ruby structure peculiarities derived from X-ray diffraction data localization of chromium atoms and electron deformation density, Phys. Status Solidi. 87 (1985) 425–433. https://doi.org/10.1002/pssa.2210870204.

[26] (COD ID:1541662) - N.C. Tombs, H.P. Rooksby, Structure of Monoxides of some Transition Elements at Low Temperatures, Nature. 165 (1950) 442–443. https://doi.org/10.1038/165442b0.

[27] (COD ID:1538531) - W.L.Roth, The magnetic structure of Co3O4, J. Phys. Chem. Solids. 25 (1964) 1–10. https://doi.org/10.1016/0022-3697(64)90156-8.

[28] (COD ID:9005204) - H.S.C. O'Neill, Temperature dependence of the cation distribution in CoAl2O4 spinel, Eur. J. Mineral. 6 (1994) 603–610. https://doi.org/10.1127/ejm/6/5/0603.

[29] O.O. James, S. Maity, Temperature programme reduction (TPR) studies of cobalt phases in -alumina supported cobalt catalysts, J. Pet. Technol. Altern. Fuels. 7 (2016) 1–12.

[30] I.G. Casella, M. Gatta, Study of the electrochemical deposition and properties of cobalt oxide species in citrate alkaline solutions, J. Electroanal. Chem. 534 (2002) 31–38. https://doi.org/10.1016/S0022-0728(02)01100-2.

Figure captions

Fig. 1. The particle size distribution of **a)** initial oxides of Co_3O_4 and Al_2O_3 and **b)** binary mixtures of samples with different percentage of Co content obtained by mechanochemical synthesis.

Fig. 2. X-ray diffractograms of the starting commercial powders of alumina and cobalt oxide

Fig. 3. XRD pattern of samples: a) with different cobalt contents after 60 min grinding and b) deconvolution of the part of the spectrum with the most intense line of cobalt spinels (Co_3O_4 and/or $CoAl_2O_4$) (A-alumina, C-cobalt spinel)

Fig. 4. TPR profiles of the investigated samples (1–Al_2O_3, 2–4%Co_3O_4-A, 3–4%$CoAl_2O_4$-A, 4–8%$CoAl_2O_4$-A, 5–16%$CoAl_2O_4$-A)

Fig. 5. a) Comparison of stable cyclic voltammograms of CP-Al_2O_3 (dot line) CP-4%Co_3O_4-A (black line) and CP-4%$CoAl_2O_4$-A (gray line), b) First (dashed line) and stable (solid line) cyclic voltammograms of CP-4%Co_3O_4-A, and c) CP-4%$CoAl_2O_4$-A in 1 M NaOH (with enlarged scale ×6)

Fig. 6. Stable cyclic voltammograms of CP-x%$CoAl_2O_4$-A in 1 M NaOH: CP-4%$CoAl_2O_4$-A (dash), CP-8%$CoAl_2O_4$-A (solid), CP-16%$CoAl_2O_4$-A (dot).

Fig. 7. Bode plots of CP-4%Co_3O_4-A (solid line) and CP-4%$CoAl_2O_4$-A (dashed line) recorded in 1 M NaOH at +0.4 V

Fig. 8. CVs of a) CP-Al_2O_3 (enlarged ×400), b) CP-4%Co_3O_4-A, and c) CP-4%$CoAl_2O_4$-A in the absence (dashed line) and presence (solid line) of 5mM glucose in 1M NaOH solution.

Fig. 9. a) Chronoamperometric response of the CP-4%Co_3O_4 (black curve) and CP-4%$CoAl_2O_4$ (grey curve) after successive additions of glucose to 1 M NaOH at the applied potential +0.45 and b) corresponding data fitted with curve given in Eq. 4

Fig. 10. a) Chronoamperometric response after successive additions of glucose to 1 M NaOH at the applied potential +0.45 for different electrodes and b) corresponding data and fitting curves of CP-4%$CoAl_2O_4$-A (light grey), CP-8%$CoAl_2O_4$-A (grey) and CP-16%$CoAl_2O_4$-A (black).

Figures

Fig. 1a

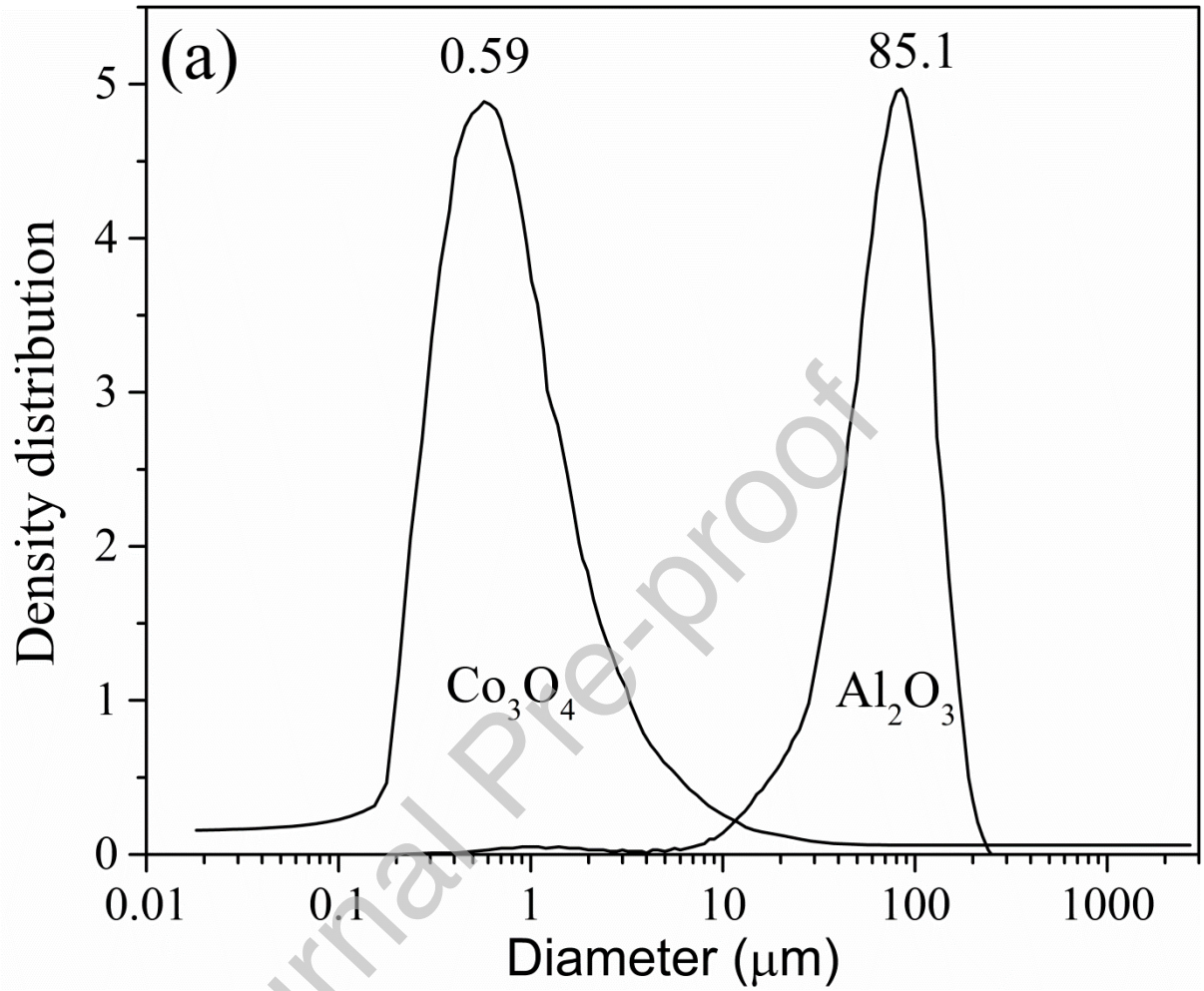

Fig. 1b

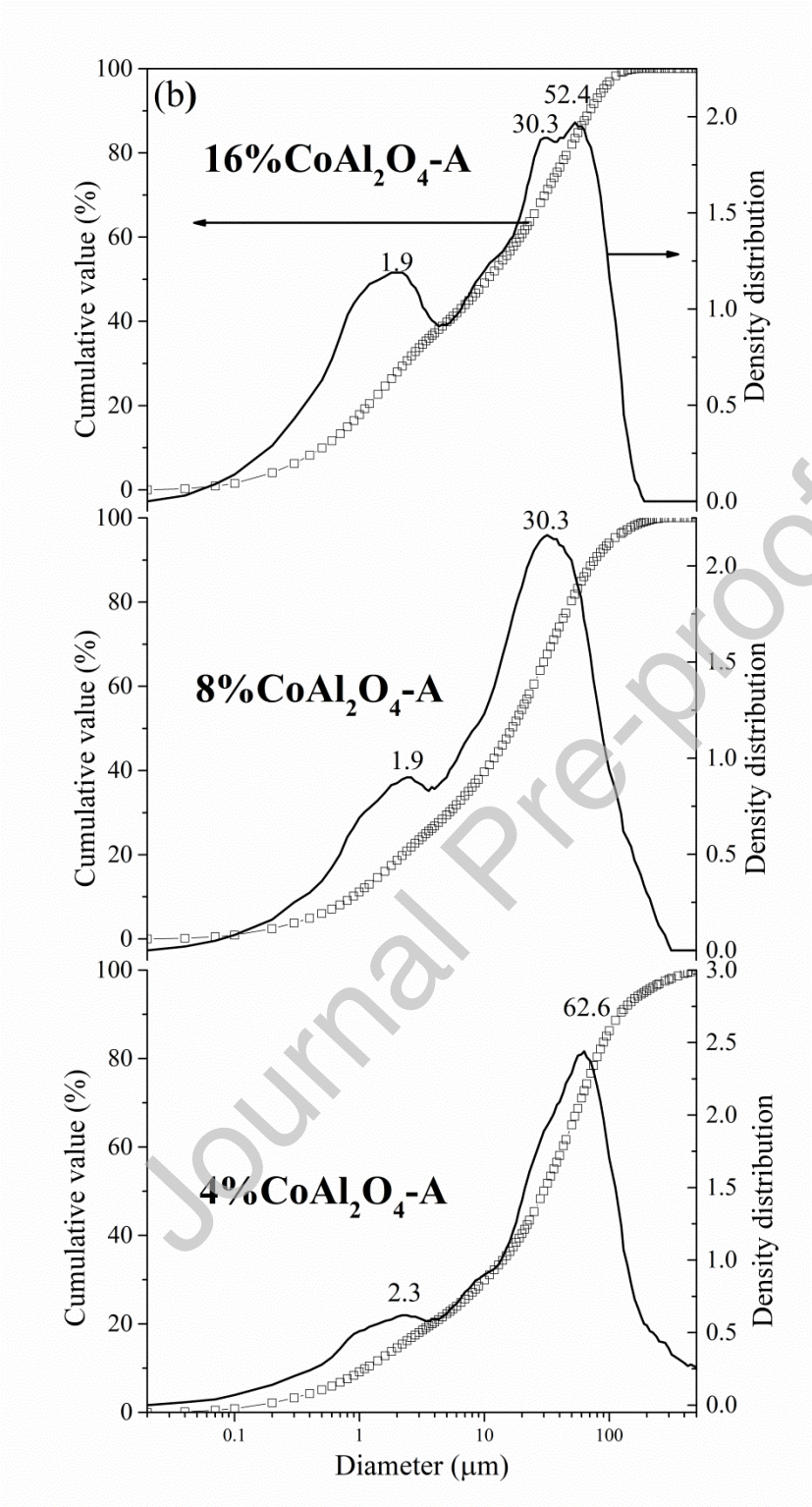

Fig. 2

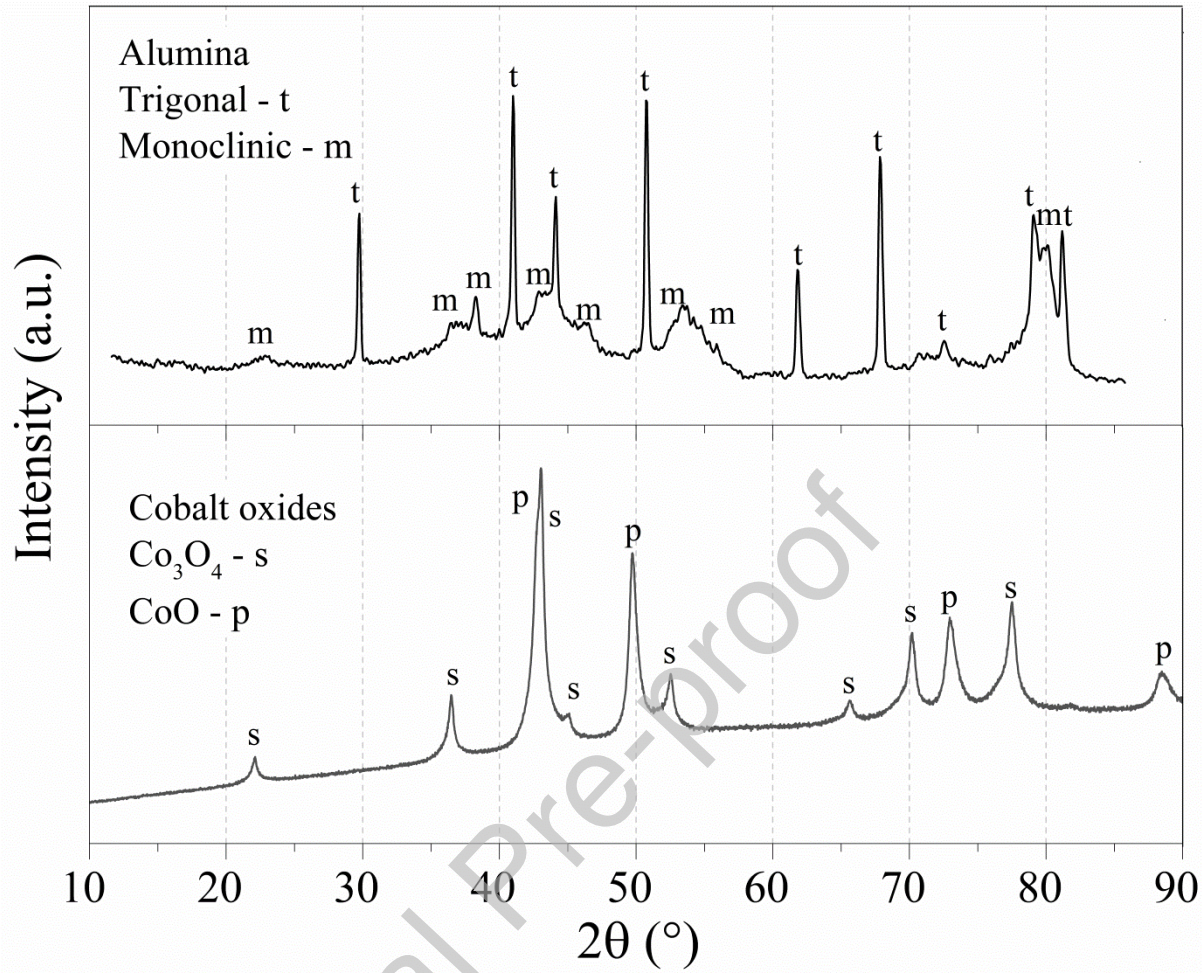

Fig. 3

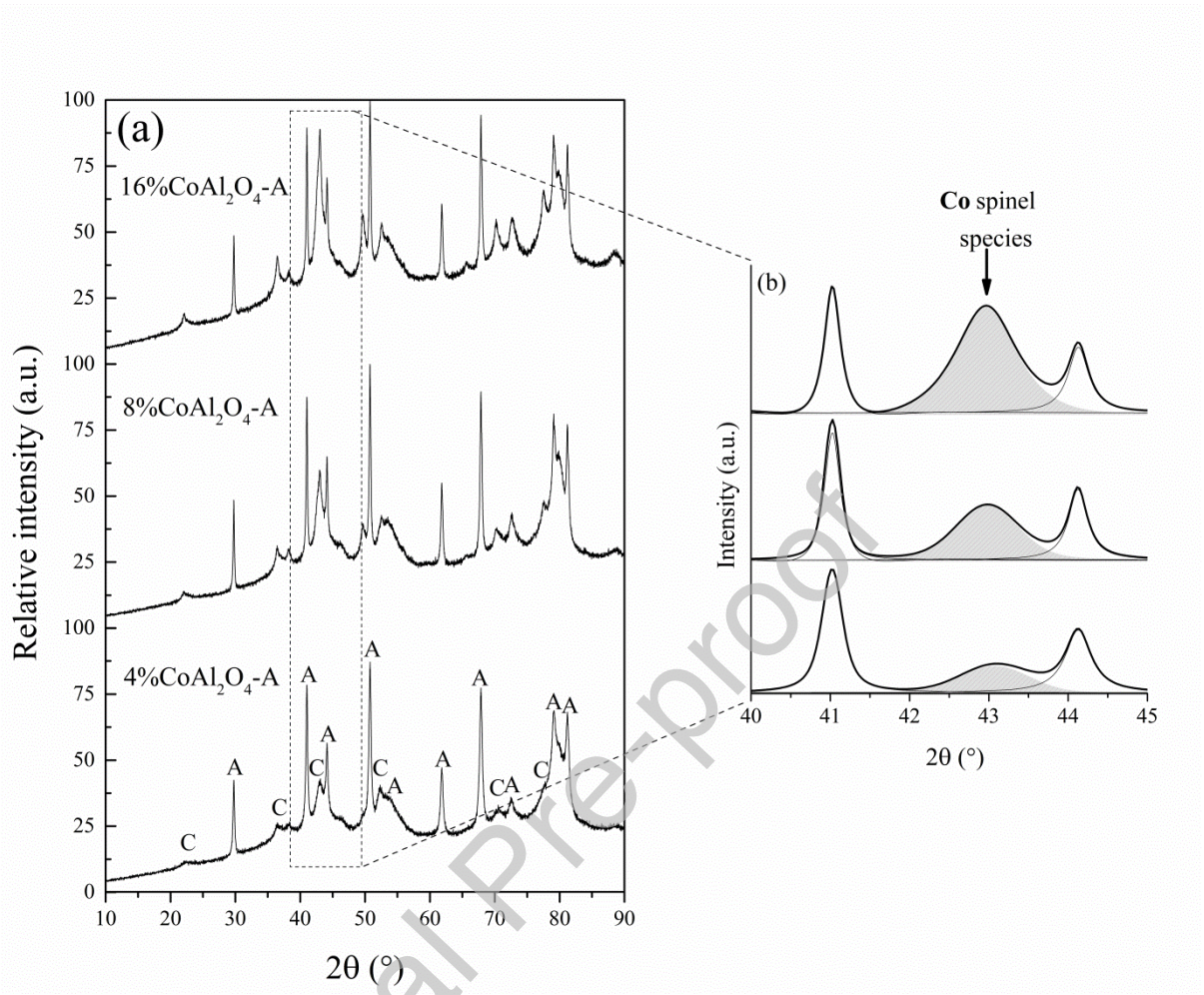

Fig. 4

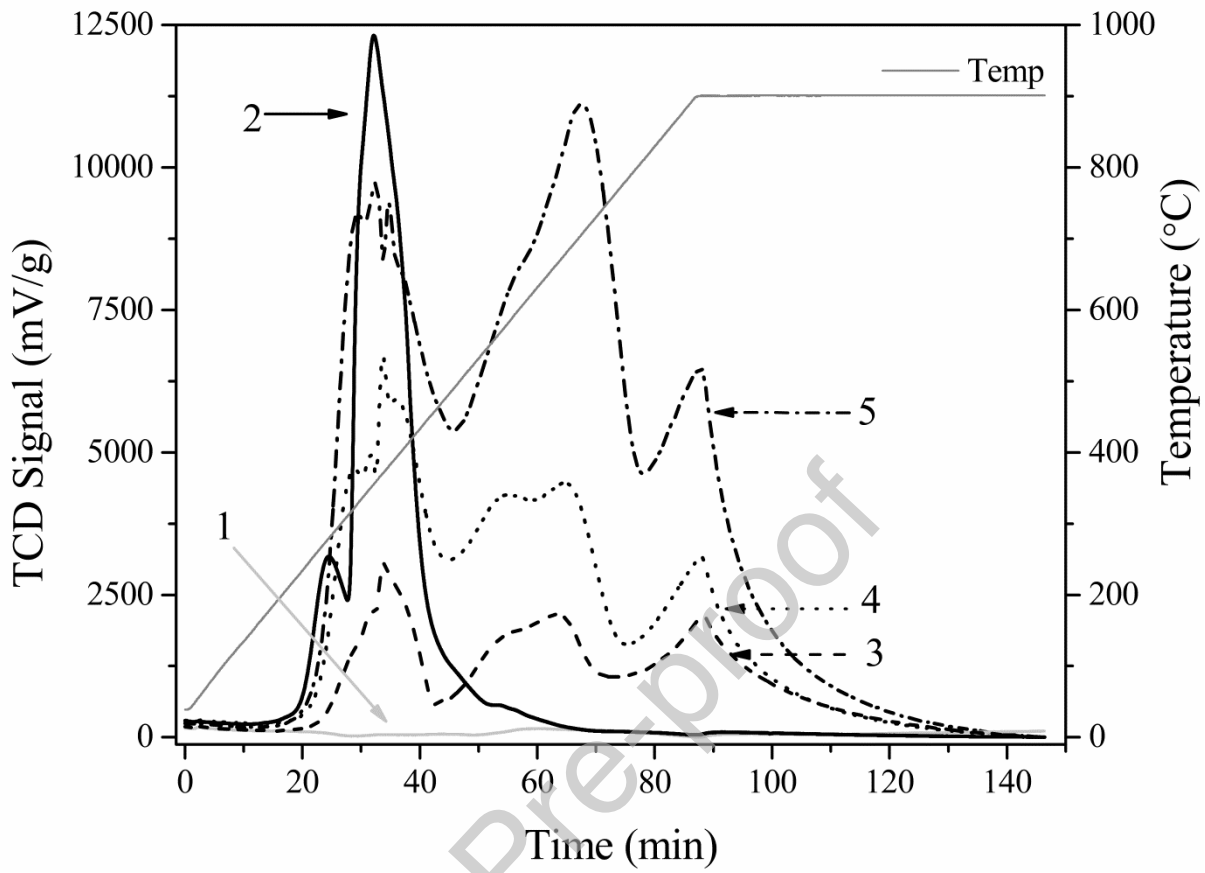

Fig. 5a

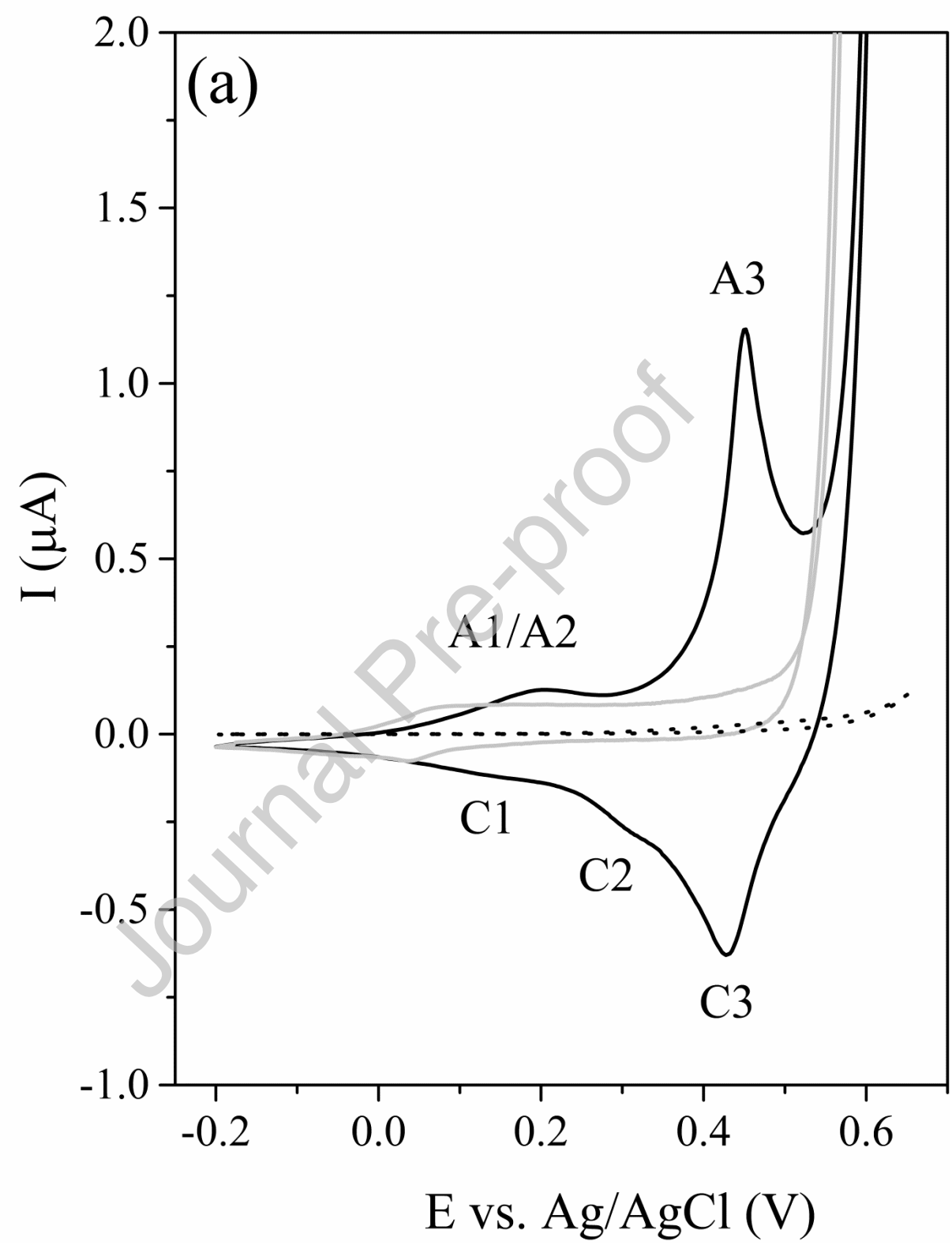

Fig. 5b

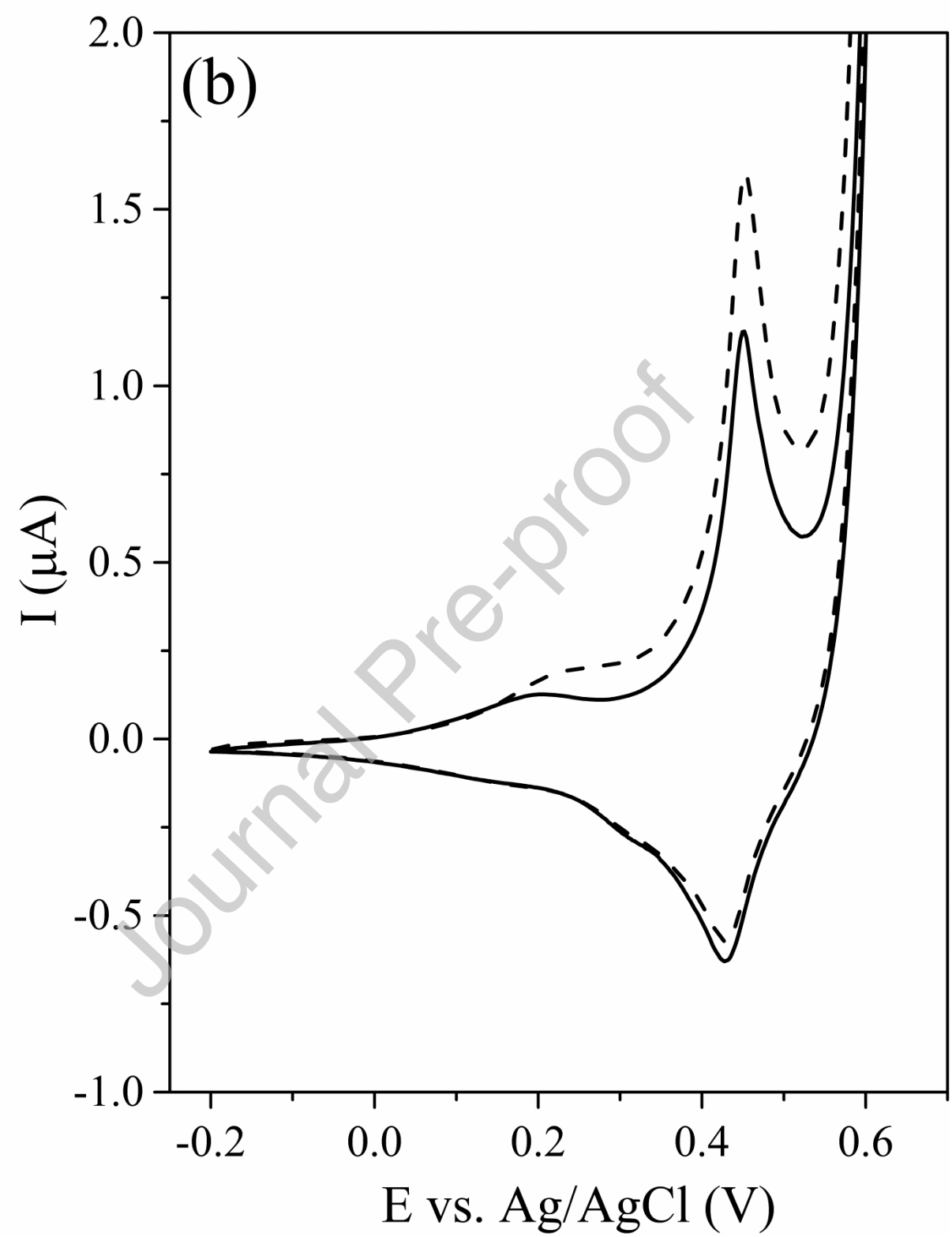

Fig. 5c

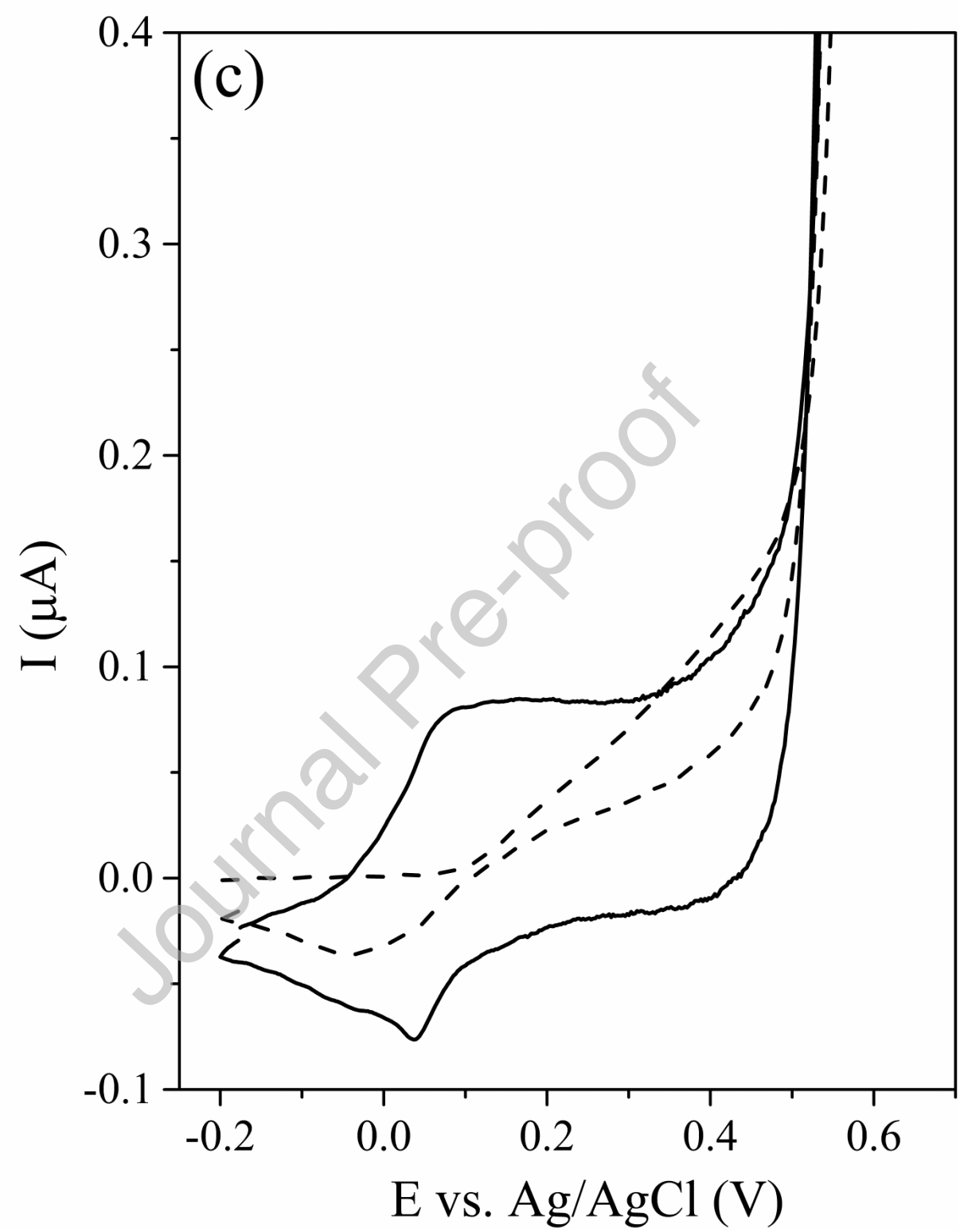

Fig. 6

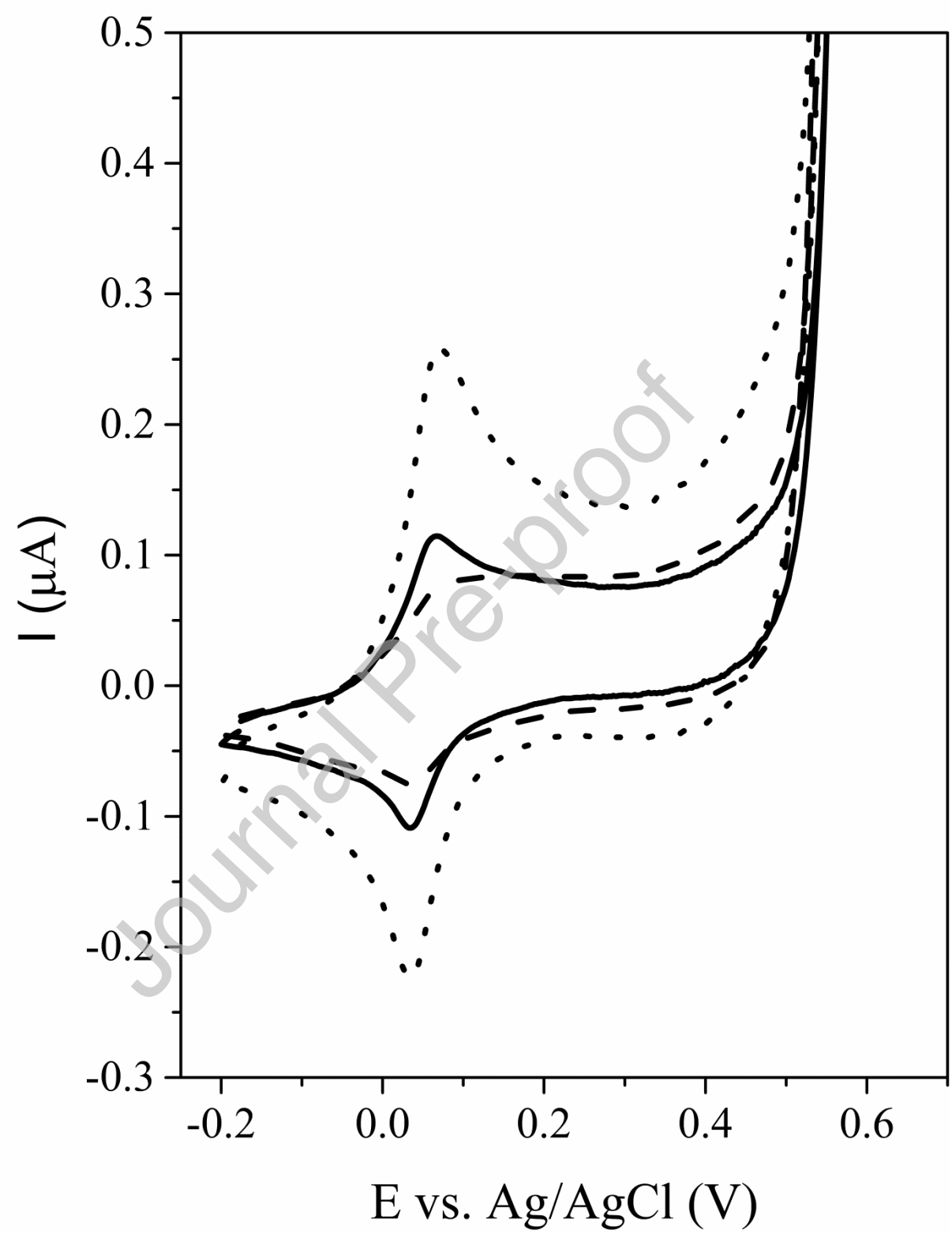

Fig. 7

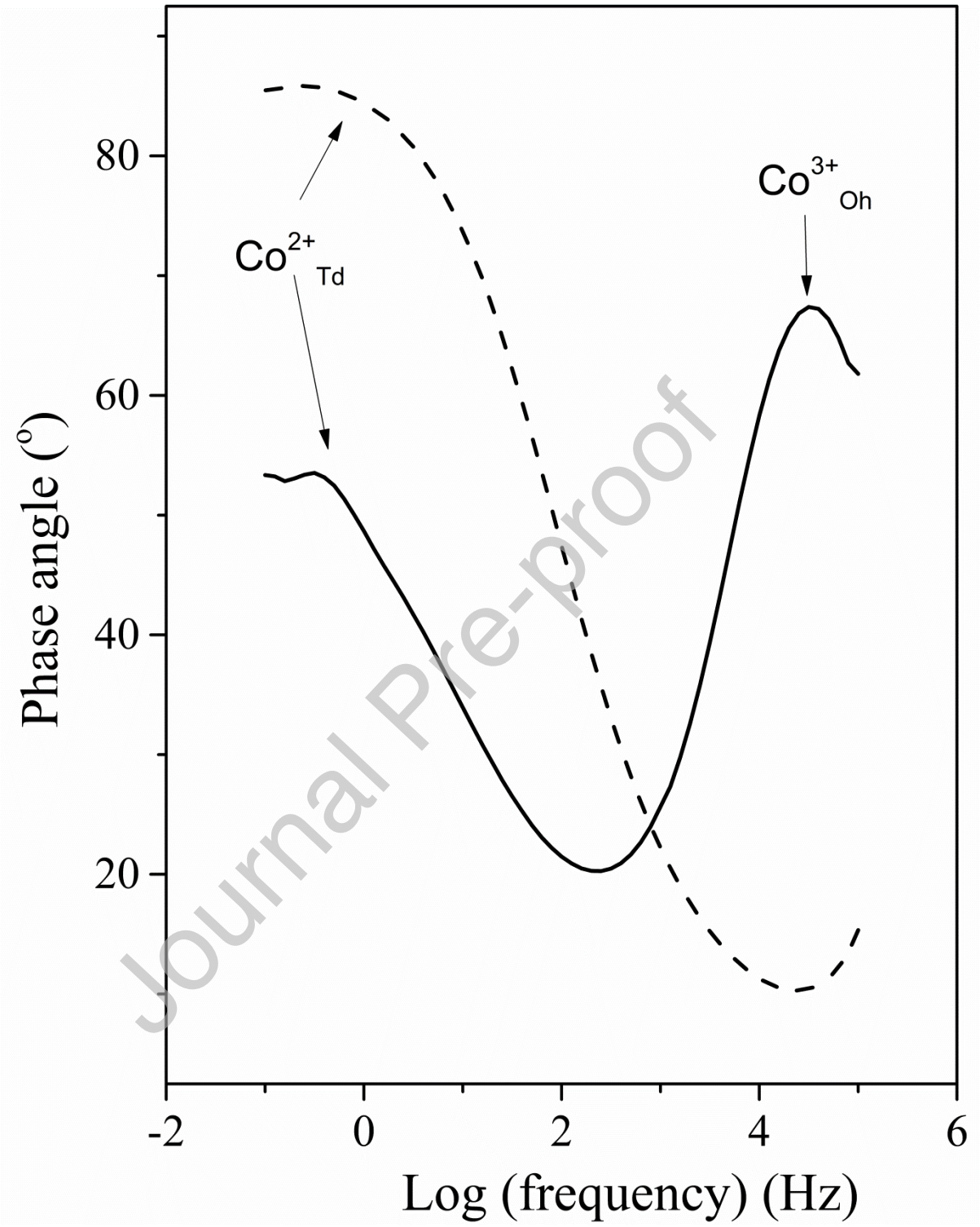

Fig. 8a

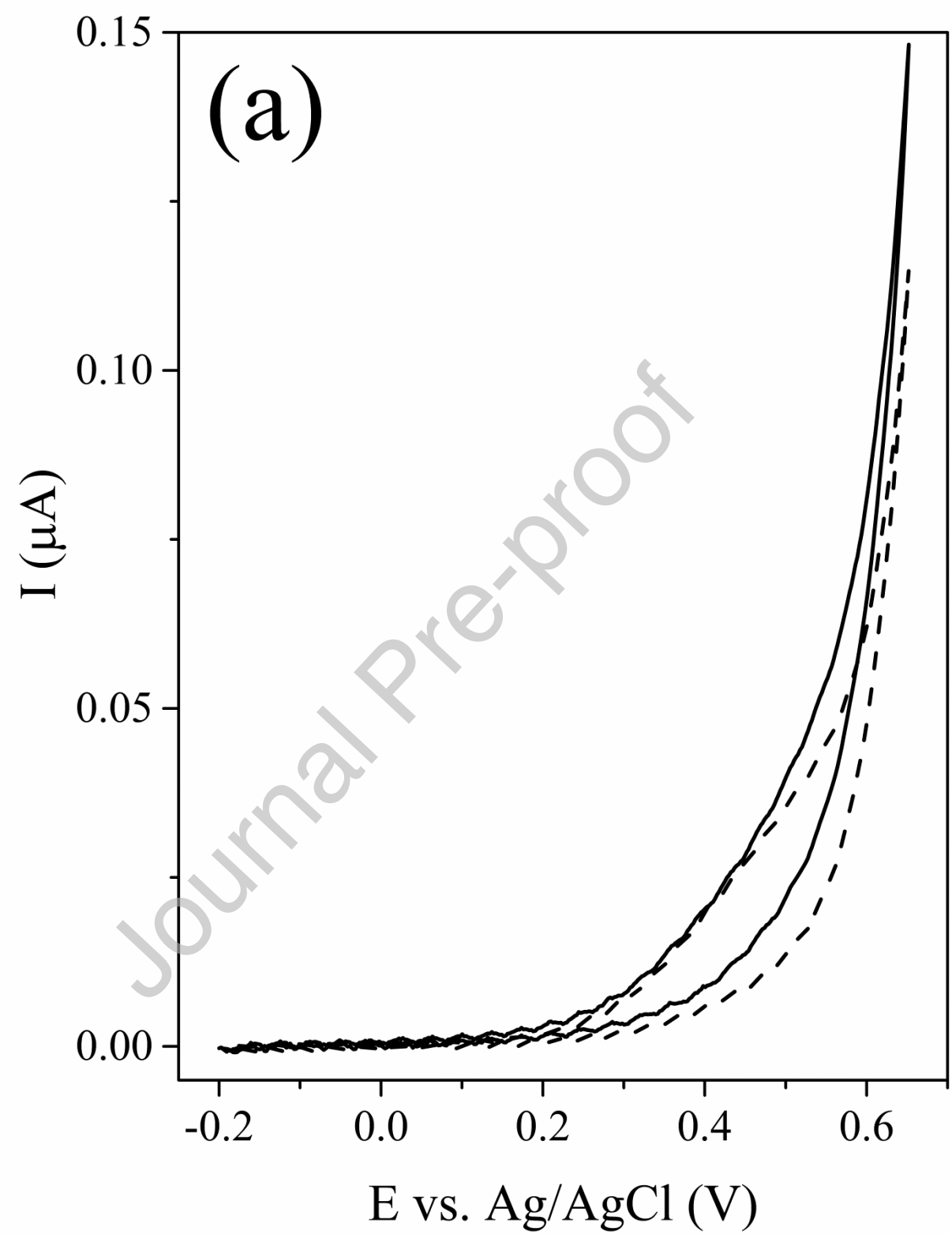

Fig. 8b

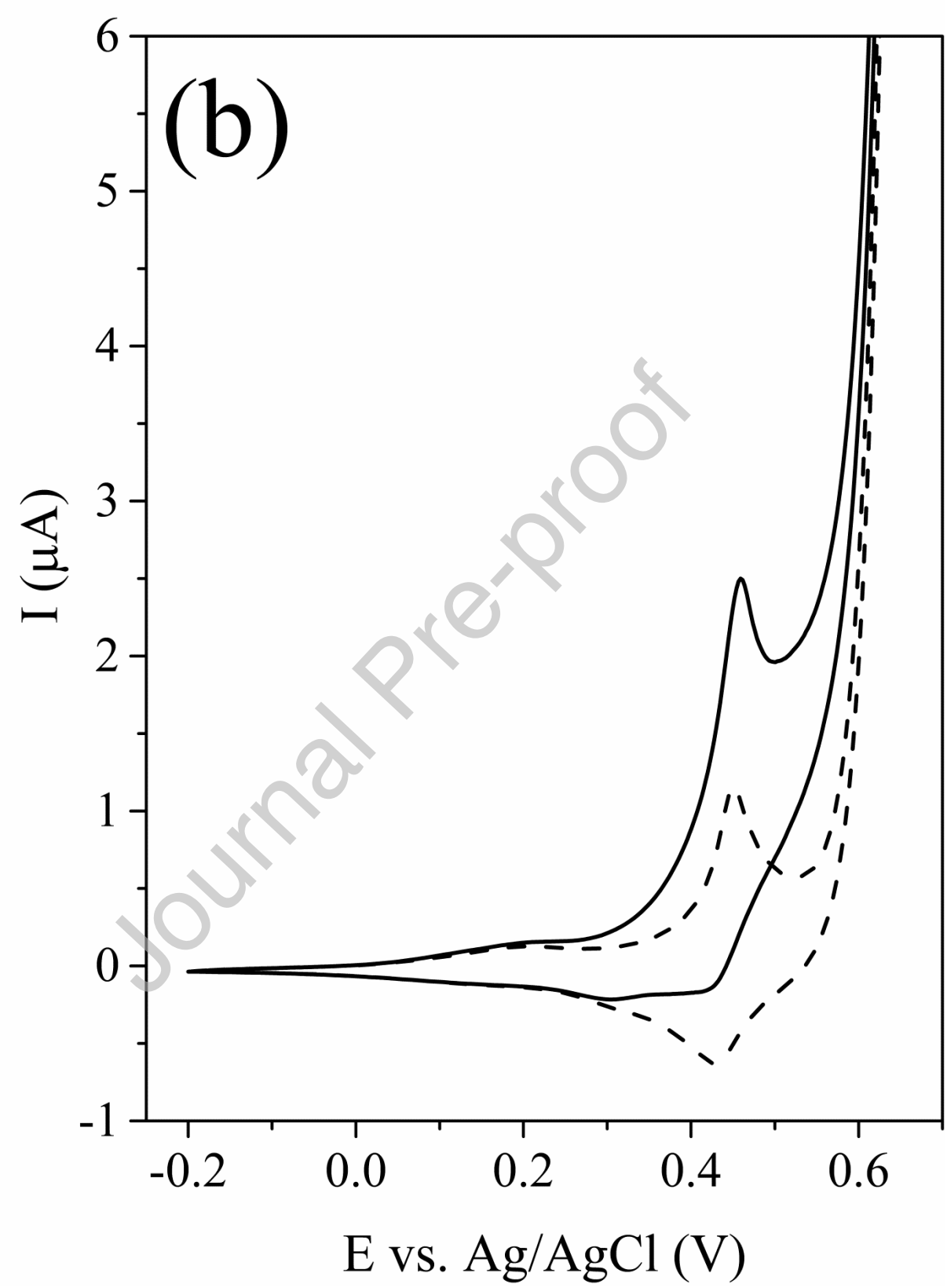

Fig. 8c

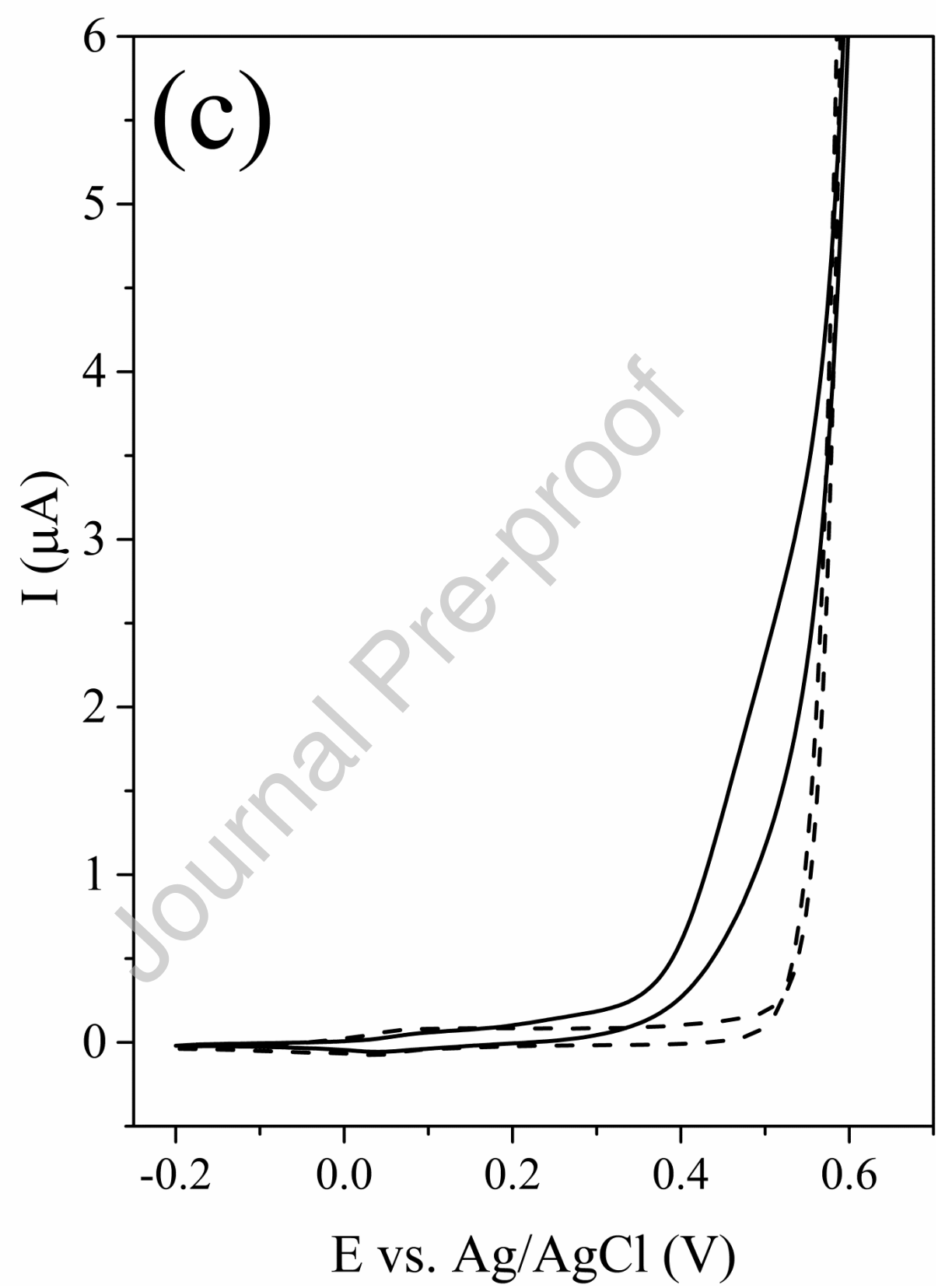

Fig. 9a

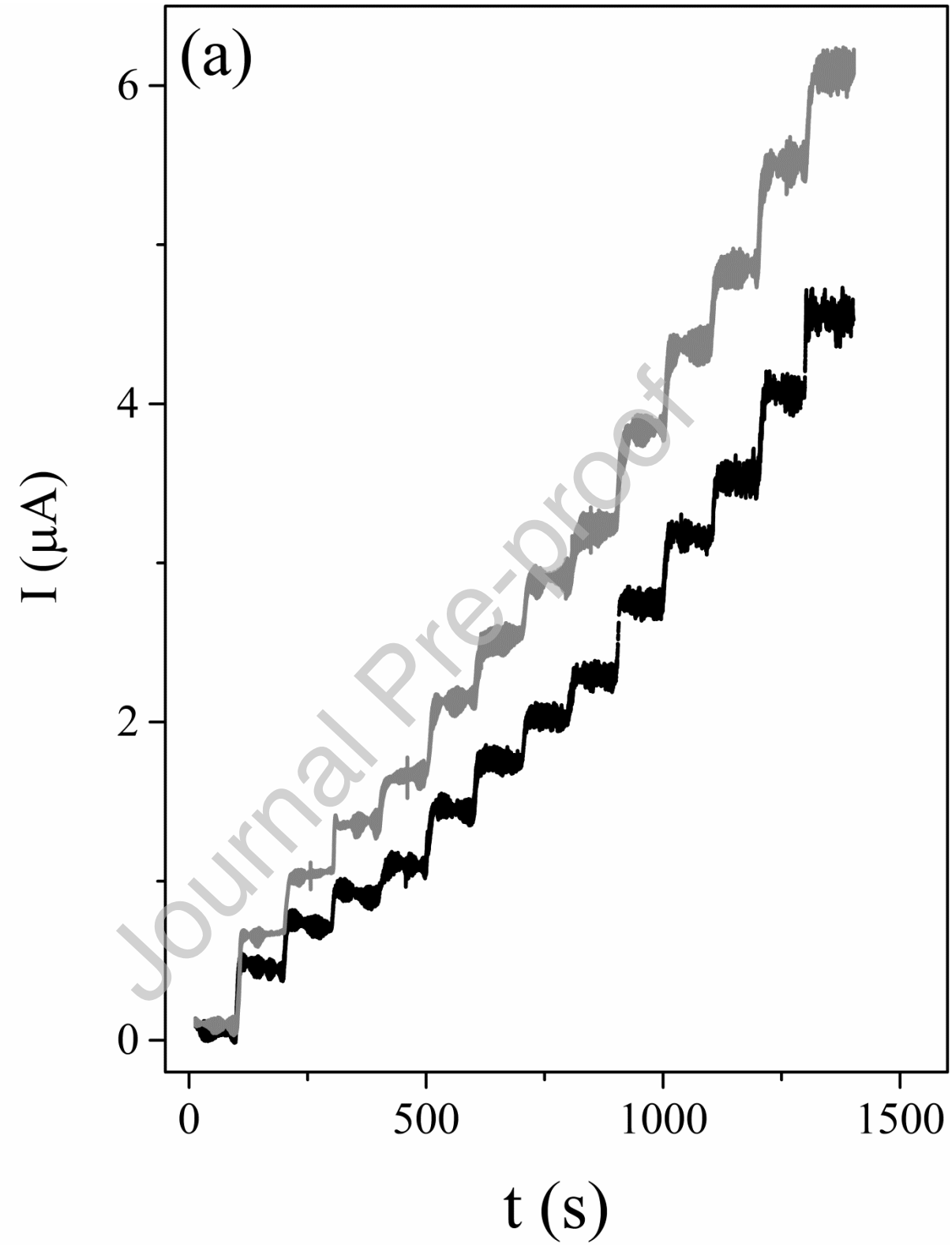

Fig. 9b

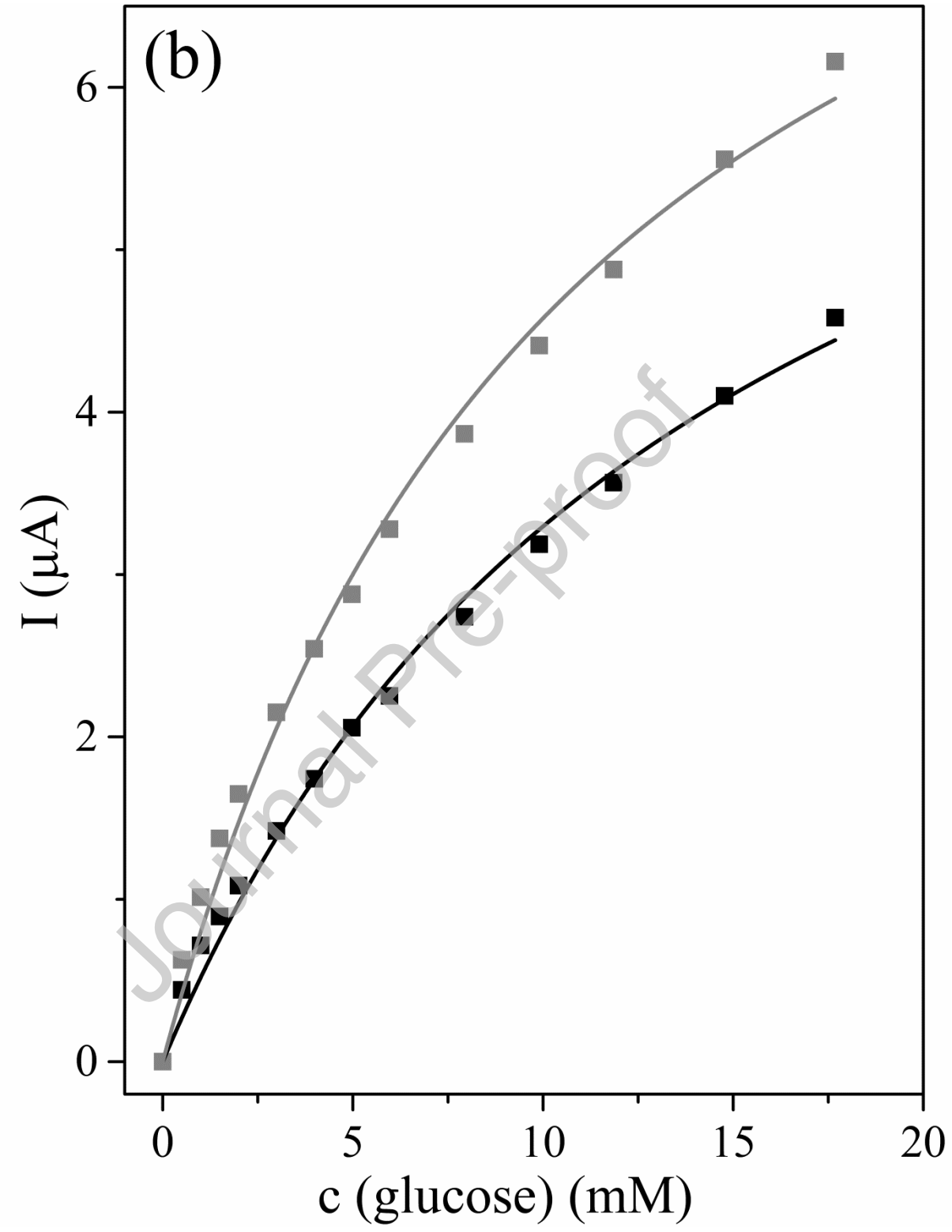

Fig. 10a

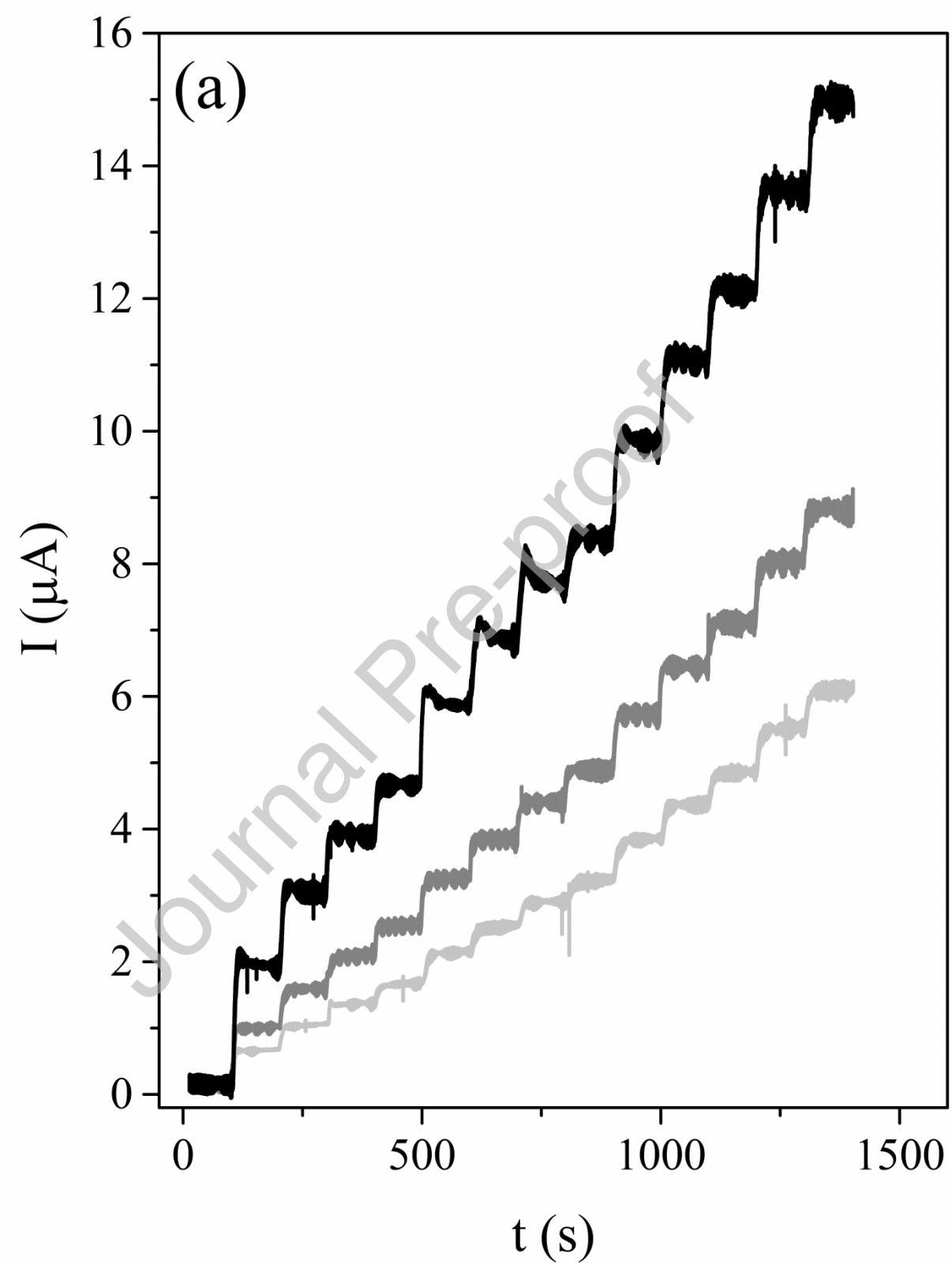

Fig. 10 b

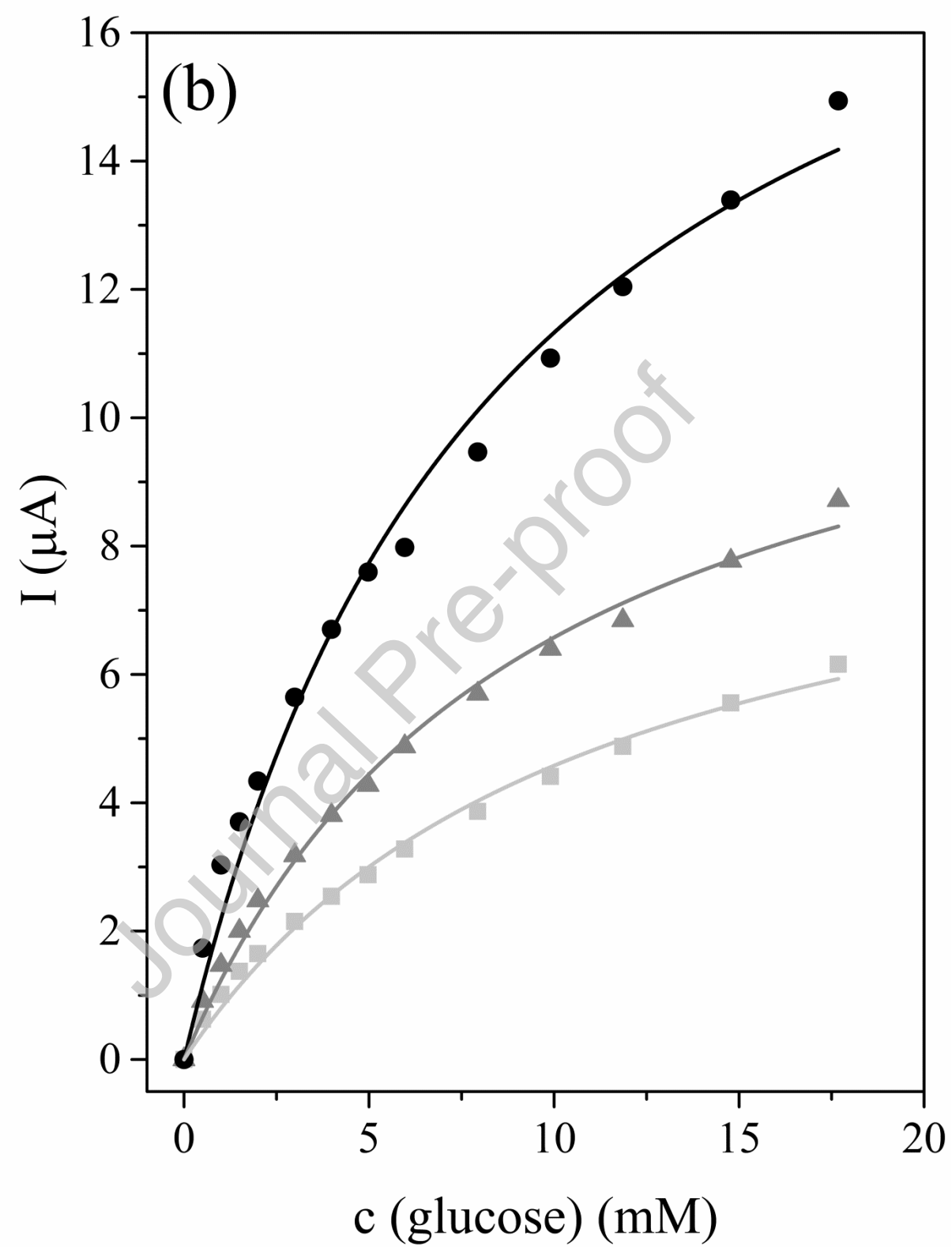

Graphical abstract